Gain Compression and Thermal Analysis of a Sapphire-Bonded Photonic Crystal Microcavity Laser

Ling Lu, Adam Mock, Mahmood Bagheri, Jiang-Rong Cao, Sang-Jun Choi, John O'Brien, and P. Daniel Dapkus

***Abstract*—Gain compression factor and thermal properties of a photonic crystal microcavity laser bonded on a sapphire substrate are extracted by analyzing wavelength shifts under different duty cycles. A high thermal resistance of 43 K/mW and a gain compression factor of 1.2×10^{-16} cm^3 are obtained.**

***Index Terms*—Continuous wave (CW), duty cycle, gain compression, microcavity laser, photonic crystal (PhC), thermal resistance.**

I. INTRODUCTION

A room-temperature (RT) two-dimensional photonic crystal (PhC) microcavity laser with high modulation bandwidth is a good on-chip source candidate for photonic integrated circuits. However, poor heat dissipation prevents most of those lasers from RT continuous-wave (CW) operation [1], [2]. In addition, gain compression is a very important factor in high-speed lasers [3]. Gain compression is well known to dampen the relaxation oscillations and limit a laser's bandwidth. The introduction of a sapphire substrate allowed our PhC microcavity lasers to operate under RT CW conditions [4] and achieve a direct modulation bandwidth of more than 10 GHz [5], [6]. In this letter, we extract coefficients related to the thermal properties and gain compression factor by analyzing the wavelength shifts under various duty cycles.

II. MEASUREMENT OF WAVELENGTH SHIFT

Fig. 1 is a scanning electron microscope (SEM) image showing a finished device patterned on a 240-nm-thick InGaAsP membrane bonded on a sapphire substrate. These cavities were formed by removing four periods of air holes in a hexagonal shape (D4 cavity) in the otherwise perfect trigonal PhC lattice. The membrane waveguide was grown by metal–organic chemical vapor deposition. It contains four 0.6% compressively strained 10-nm-thick InGaAsP quantum wells (QWs), whose emission wavelength is near 1.55 μm, and 20-nm-thick InGaAsP barrier layers between the QWs, whose emission wavelength is 1.25 μm [7]. The fabrication processes, characterization setup are detailed in the previous publications [4], [8]. An 852-nm diode laser is used to pump the device with about 2-μm spot size. Its pulsewidth (t_1) was fixed at 8 ns. A cavity with 390-nm lattice constant and 0.355 hole radius to lattice constant ratio was used in this study and all the measurements were done at a 21 °C substrate temperature. The wavelength is monitored in an optical spectrum analyzer with 0.1-nm resolution bandwidth.

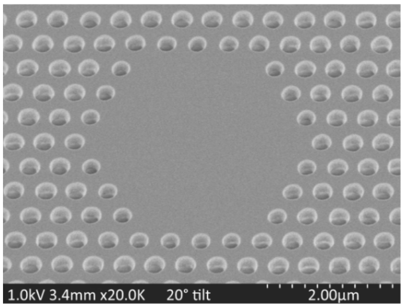

Fig. 1. SEM image of a fabricated D4 cavity on a sapphire substrate.

The CW light-in–light-out (L-L) curve in Fig. 2(a) starts to roll over at about four times the CW threshold. The blue and red shifts of the resonant wavelengths, illustrated in Fig. 2(a), as a function of pump power are a result of increasing carrier density and increasing device temperature which move the refractive index in opposite directions. Processes such as thermal expansion [9] and thermal strain-induced index change [10] are negligible compared to the two mentioned. Below threshold, the increase of carrier density is dominant and the wavelengths blueshift; above threshold, the wavelength shifts from carrier density and device temperature are comparable. The laser redshifts under CW condition and blueshifts under pulsed conditions, since device heating is alleviated as the duty cycle decreases. For the same reason, laser threshold decreases with the decrease of duty cycle.

The existence of the blue shift above threshold is a sign that the carrier density is not clamped and is modeled through gain compression. This can be verified by the growing intensity of spontaneous emission with increasing pump power away from the lasing wavelength above threshold shown in Fig. 2(b). Low intensity PL of the QW is also plotted for comparison.

III. MODELING OF WAVELENGTH SHIFT

In order to quantify the contribution to the wavelength shift from both temperature (T) and carrier density (N) in (1)

$$\Delta\lambda = (\partial\lambda/\partial n)[(\partial n/\partial T)\Delta T + (\partial n/\partial N)\Delta N] \qquad (1)$$

the device heating was modeled analogously to an *RC* circuit and the carrier density is modeled using the phenomenological parameter (ε), known as the gain compression factor. Here n is the refractive index of the semiconductor slab. The coefficients $\partial n/\partial T$ $(2.5 \times 10^{-4\circ}\mathrm{C}^{-1})$ and $\partial n/\partial N$ $(-1.63 \times 10^{-20}$ cm$^3)$ can be found in [11] and [12], respectively. $\partial\lambda/\partial n$ is estimated through numerical modeling in Section IV.

Manuscript received February 20, 2009; revised April 29, 2009. First published June 02, 2009; current version published August 12, 2009. This work was supported by the National Science Foundation under Grant ECS-0507270.

The authors are with the Department of Electrical Engineering (Electrophysics Division), University of Southern California, Los Angeles, CA 90089 USA (e-mail: lingl@usc.edu; amock@usc.edu; mbagheri@usc.edu; jiangrongcao@yahoo.com; sangjun.choi@yahoo.com; jdobrien@usc.edu; dapkus@usc.edu).

Color versions of one or more of the figures in this letter are available online at http://ieeexplore.ieee.org.

Digital Object Identifier 10.1109/LPT.2009.2023228

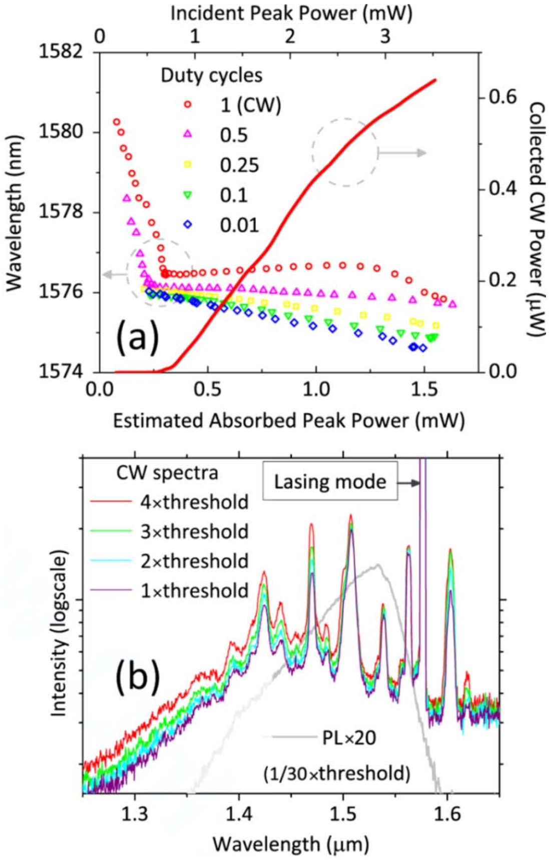

Fig. 2. (a) Wavelength versus pumping power of the same lasing mode under different duty cycles. L-L curve under CW condition is also included. (b) CW lasing spectra under various pumping levels and the photoluminescence (PL) of gain material at low bias.

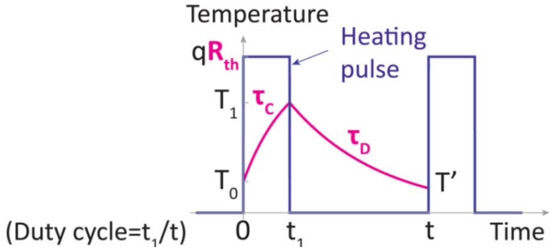

Fig. 3. Illustration of the "*RC* circuit" thermal model.

Fig. 3 illustrates our analytical thermal model. The device temperature is "charged" and "discharged" with time constants (τ_C) and (τ_D) by the heating pulse qR_{th}, where R_{th} is the thermal resistance and q is the heat flux from photopumping. It is assumed that all nonradiative recombination contributes to heat. The radiative efficiency is estimated to be 64% below threshold and 95% above threshold [13]. The average temperature increase can thus be expressed in (2) as a function of absorbed pumping power and duty cycles (dc) at steady state when T_0 equals T'

$$\Delta T_{\text{average}} = qR_{\text{th}}\left[1+(\tau_C/t_1) \times \frac{1-e^{(1/\text{dc}-1)(t_1/\tau_D)}}{e^{(1/\text{dc}-1)(t_1/\tau_D)}-e^{(-t_1/\tau_C)}}\left(1-e^{-t_1/\tau_C}\right)\right]. \quad (2)$$

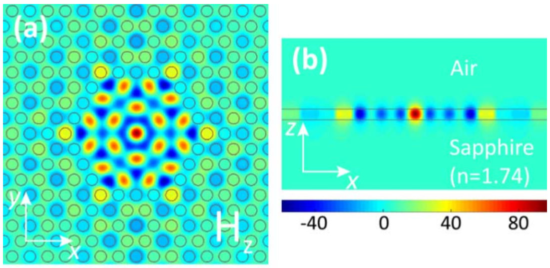

Fig. 4. H_z field component of the lasing mode calculated by 3-D FDTD. (a) Field distribution in $x-y$ plane at the mid-plane of the membrane. (b) Field distribution in the $x-z$ plane through the center of the cavity. The air hole and membrane edges are outlined in gray.

The increase of the carrier density above threshold can be found by equating QW gain (g) to the total optical loss which was assumed to be a constant above threshold for all duty cycles. The QW gain as a function of carrier density and photon density (N_p) is expressed as $g(N, N_p) = g_0 \ln(N/N_{\text{transparency}})/(1+\varepsilon N_p)$. Thus,

$$\begin{aligned}\Delta N_{\text{slab}} &= f_{\text{QW}}\Delta N_{\text{QW}} \\ &= f_{\text{QW}}\left[N_{\text{threshold}}\left(e^{\varepsilon N_p \ln(N_{\text{threshold}}/N_{\text{transparency}})}-1\right)\right] \quad (3)\end{aligned}$$

where f_{QW} is a conversion factor from QW carrier density to the averaged carrier density in the semiconductor slab. Since the carrier density inside the QWs is higher than that in the barriers, f_{QW} is less than 1.

Equations (1)–(3) with the assumptions of constant $N_{\text{threshold}}$ and ε for all duty cycles complete our model. $\tau_C, \tau_D, R_{\text{th}}, \varepsilon$ and f_{QW} can thus be determined by fitting all five curves of wavelength data in Fig. 2(a) simultaneously.

IV. 3-D FDTD SIMULATION

The three-dimensional finite-difference time-domain (3-D FDTD) method was used to model the electromagnetic field in this cavity. Mode identification was carried out the same way as that in [14]. The midplane field distribution of the lasing mode is plotted in Fig. 4. The passive quality (Q) factor is 1732, which is in reasonable agreement with the estimated Q value (1250) from threshold carrier density [8], [15] considering the imperfections in fabrication and optical absorption loss [15]. The mode volume is evaluated to be $17.8(\lambda/n)^3$ [16], where n is 3.4 in the calculation. In order to obtain $\partial\lambda/\partial n$ for this mode, we varied, in the simulation, the refractive index of the slab at the center region of the cavity. The diameter of this region is 3 μm. By monitoring the linear shift of the resonant peak with the change of the index, we get 210 nm for $\partial\lambda/\partial n$.

V. RESULTS OF DATA FITTING

Our model provides a good fit to the experimental wavelength data as shown in Fig. 5(a). Fig. 5(b) plots, according to the fit, both carrier density and device temperature as a function of pump power for all duty cycles. When the CW pumping level exceeds four times the CW threshold where the CW L-L curve is beginning to roll over, the rate of blue shift is much faster

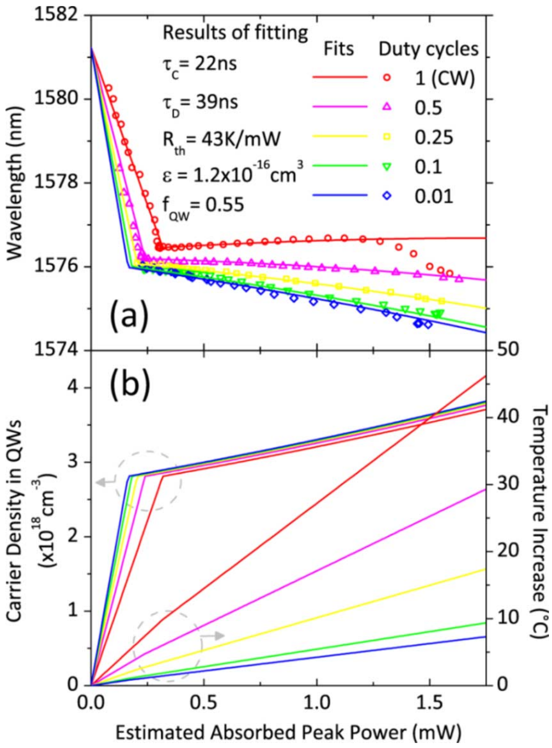

Fig. 5. (a) Experimental wavelength data fitted by our model. (b) Carrier density and temperature behaviors as a result of the fit.

than what the model predicts. This indicates a different mechanism responsible for the rapid growth of carrier density at about 32 °C above RT and is likely due to the increase of nonradiative recombination rates and the decrease of QW gain with the rise of laser temperature. The standard deviation of the fit, excluding this high CW bias region, is 0.1 nm. The results of the total number of five fitting parameters are listed in Fig. 5(a). A very high thermal resistance of 43 K/mW is obtained due to localized heating and insufficient heat dissipation. The gain compression factor of 1.2×10^{-16} cm^3 agrees very well with the reported and predicted values for strained QW lasers [17]–[19].

VI. CONCLUSION

We measured, under various duty cycles, the wavelength behaviors of a sapphire-bonded RT CW QW PhC microcavity laser. Changes in carrier density and device temperature from photopumping are responsible for the wavelength shifts. We modeled carrier density above threshold with gain compression factor and device temperature through an *RC* circuit analogy. Fitting the data using our model provides both thermal properties and gain compression factor of the laser.

ACKNOWLEDGMENT

The authors would like to thank L. Stewart at the University of Southern California for his help on fabrication.

REFERENCES

[1] J. K. Hwang, H. Y. Ryu, D. S. Song, I. Y. Han, H. K. Park, D. H. Jang, and Y. H. Lee, "Continuous room-temperature operation of optically pumped two-dimensional photonic crystal lasers at 1.6 μm," *IEEE Photon. Technol. Lett.*, vol. 12, no. 10, pp. 1295–1297, Oct. 2000.

[2] K. Nozaki, S. Kita, and T. Baba, "Room temperature continuous wave operation and controlled spontaneous emission in ultrasmall photonic crystal nanolaser," *Opt. Express*, vol. 15, pp. 7506–7514, 2007.

[3] E. K. Lau, A. Lakhani, R. S. Tucker, and M. C. Wu, "Enhanced modulation bandwidth of nanocavity light emitting devices," *Opt. Express*, vol. 17, pp. 7790–7799, 2009.

[4] J. R. Cao, W. Kuang, Z. J. Wei, S. J. Choi, H. X. Yu, M. Bagheri, J. D. O'Brien, and P. D. Dapkus, "Sapphire-bonded photonic crystal microcavity lasers and their far-field radiation patterns," *IEEE Photon. Technol. Lett.*, vol. 17, no. 1, pp. 4–6, Jan. 2005.

[5] M. Bagheri, M. H. Shih, Z. J. Wei, S. J. Choi, J. D. O'Brien, P. D. Dapkus, and W. K. Marshall, "Linewidth and modulation response of two-dimensional microcavity photonic crystal lattice defect lasers," *IEEE Photon. Technol. Lett.*, vol. 18, no. 10, pp. 1161–1163, May 15, 2006.

[6] M. Bagheri, M. Shih, S. Choi, J. O'Brien, and P. Dapkus, "Effect of carrier capture on modulation response properties of semiconductor microdisk lasers," in *Proc. LEOS*, Newport Beach, CA, 2008, Paper WQ2.

[7] A. Mathur and P. D. Dapkus, "Fabrication, characterization and analysis of low threshold current density 1.55 μm strained quantum-well lasers," *IEEE J. Quantum Electron.*, vol. 32, no. 2, pp. 222–226, Feb. 1996.

[8] M. H. Shih, W. Kuang, T. Yang, M. Bagheri, Z. J. Wei, S. J. Choi, L. Lu, J. D. O'Brien, and P. D. Dapkus, "Experimental characterization of the optical loss of sapphire-bonded photonic crystal laser cavities," *IEEE Photon. Technol. Lett.*, vol. 18, no. 3, pp. 535–537, Feb. 1, 2006.

[9] P.-T. Lee, J. R. Cao, S.-J. Choi, Z.-J. Wei, J. D. O'Brien, and P. D. Dapkus, "Operation of photonic crystal membrane lasers above room temperature," *Appl. Phys. Lett.*, vol. 81, pp. 3311–3313, 2002.

[10] A. Jansen van Doom, M. van Exter, and J. Woerdman, "Strain-induced birefringence in vertical-cavity semiconductor lasers," *IEEE J. Quantum Electron.*, vol. 34, no. 4, pp. 700–706, Apr. 1998.

[11] N. Cherroret, A. Chakravarty, and A. Kar, "Temperature-dependent refractive index of semiconductors," *J. Mater. Sci.*, vol. 43, pp. 1795–1801, 2008.

[12] J. P. Weber, "Optimization of the carrier-induced effective-index change in InGaAsP waveguides," *IEEE J. Quantum Electron.*, vol. 30, no. 8, pp. 1801–1816, Aug. 1994.

[13] L. Lu, A. Mock, T. Yang, M. H. Shih, E. H. Hwang, M. Bagheri, A. Stapleton, S. Farrell, J. O'Brien, and P. D. Dapkus, "120 μW peak output power from edge-emitting photonic crystal double-heterostructure nanocavity lasers," *Appl. Phys. Lett.*, vol. 94, p. 111101, 2009.

[14] M. H. Shih, M. Bagheri, A. Mock, S. J. Choi, J. D. O'Brien, P. D. Dapkus, and W. Kuang, "Identification of modes and single mode operation of sapphire-bonded photonic crystal lasers under continuous-wave room temperature operation," *Appl. Phys. Lett.*, vol. 90, p. 121116, 2007.

[15] L. Lu, A. Mock, M. Bagheri, E. H. Hwang, J. O'Brien, and P. D. Dapkus, "Double-heterostructure photonic crystal lasers with reduced threshold pump power and increased slope efficiency obtained by quantum well intermixing," *Opt. Express*, vol. 16, pp. 17342–17347, 2008.

[16] O. Painter, R. K. Lee, A. Scherer, A. Yariv, J. D. O'Brien, P. D. Dapkus, and I. Kim, "Two-dimensional photonic bandgap defect mode laser," *Science*, vol. 284, pp. 1819–1821, 1999.

[17] M. Willatzen, T. Takahashi, and Y. Arakawa, "Nonlinear gain effects due to carrier heating and spectral holeburning in strained-quantum-well lasers," *IEEE Photon. Technol. Lett.*, vol. 4, no. 7, pp. 682–685, Jul. 1992.

[18] S. J. Seki, T. Yamanaka, K. Yokoyama, P. Sotirelis, and K. Hess, "Theoretical-analysis of gain saturation coefficients in InP-based strained-layer quantum-well lasers," *J. Appl. Phys.*, vol. 74, pp. 2971–2973, 1993.

[19] F. Girardin, G. H. Duan, P. Gallion, A. Talneau, and A. Ougazzaden, "Experimental investigation of the relative importance of carrier heating and spectral-hole-burning on nonlinear gain in bulk and strained multi-quantum-well 1.55 μm lasers," *Appl. Phys. Lett.*, vol. 67, pp. 771–773, 1995.